Nuclear Engineering and Technology 51 (2019) 1381–1389

Contents lists available at ScienceDirect

Nuclear Engineering and Technology

journal homepage: www.elsevier.com/locate/net

Original Article

Effect of oxide film on ECT detectability of surface IGSCC in laboratory-degraded alloy 600 steam generator tubing

Tae Hyun Lee [a], Kyung Ha Ryu [a], Hong Deok Kim [b], Il Soon Hwang [c], Ji Hyun Kim [d], Min Ho Lee [e], Sungyeol Choi [e, *]

[a] Korea Institute of Machinery and Materials, 156 Gajeongbuk-ro, Yuseong, Daejeon, 34103, South Korea
[b] Central Research Institute of Korea Hydro & Nuclear Power, 1312-70 Yusengdae-ro, Yuseong, Daejeon, 34101, South Korea
[c] Department of Nuclear Engineering, Seoul National University, 1 Gwanak-ro, Gwanak-gu, Seoul, 08826, South Korea
[d] Department of Nuclear Engineering, Ulsan National Institute of Science and Technology, 50 UNIST-gil, Ulsan, 44919, South Korea
[e] Department of Nuclear and Quantum Engineering, Korea Advanced Institute of Science and Technology, 291 Daehak-ro, Yuseong-gu, Daejeon, 34141, South Korea

ARTICLE INFO

Article history:
Received 6 January 2019
Received in revised form
5 March 2019
Accepted 7 March 2019
Available online 9 March 2019

Keywords:
Stress corrosion cracking
Eddy current tests
Steam generators
PWR
Alloy 600

ABSTRACT

Stress corrosion cracking (SCC) widely found in both primary and secondary sides of steam generator (SG) tubing in pressurized water reactors (PWR) has become an important safety issue. Using eddy-current tests (ECTs), non-destructive evaluations are performed for the integrity management of SG tubes against intergranular SCC. To enhance the reliability of ECT, this study investigates the effects of oxide films on ECT's detection capabilities for SCC in laboratory-degraded SG tubing in high temperature and high pressure aqueous environment.

1. Introduction

Non-destructive evaluation and failure prediction of steam generator tubing in pressurized water reactors (PWR) are periodically performed using eddy current test (ECT) methods. Based on the results, repairs of degraded tubes or other preventive measures are applied. The reliability of integrity assessment is strongly dependent on the accuracy of ECT in detecting various types of defects formed in tubes. The current ECT practice uses standard electrical discharge machined (EDM) specimens. The most prominent defects of nozzle material and dissimilar metal joints using nuclear power plant are mainly intergranular stress corrosion cracking (IGSCC) which have the lowest crack tip opening. Therefore, EDM Notch test specimens with abnormally severe crack tip opening have limitations as specimens for non-destructive testing of IGSCC damage. EDM notches are fundamentally different from actual defects that occur in practice and may lead to underestimation of ECT results.

In order to characterize the effects of IGSCC in the presence of an oxide film on ECTs, a number of cracked tube specimens with IGSCC, similar to those found in actual plants, are needed. These specimens need to possess similar mechanical, micro-structural, and electrochemical characteristics. The manufacturing technique for this type of specimen is, however, complex and not well established. Most specimens produced by an internal pressurization method are limited to those with semi-circular crack geometries. In earlier studies attempts were made to produce the artificial flaws caused by thermal fatigue [1,2]. The crack data were validated using the results of destructive and non-destructive tests. Unfortunately, only a small fraction of the sample could be used for the actual test because the crack size was not monitored continuously during the progress of the crack. As a result, the final crack size was not controlled, which led to excessive consumption of materials and time in the process of making the specimen. The technology we have used in this study aims to overcome the limits of previous methods by developing intergranular crack formation on Alloy 600 penetration piping at room temperature.

In this work, actual cracks in SG tubes with a high surface length to depth ratio (aspect ratio), i.e., higher than 10, on both the inner

* Corresponding author.
E-mail address: sungyeolchoi@kaist.ac.kr (S. Choi).

https://doi.org/10.1016/j.net.2019.03.005

and outer surfaces of the tubes are investigated [3,4]. A radial dent loading method for introducing axial intergranular cracks with high aspect ratios is adopted. Sensitized Alloy 600 tubes are used to generate intergranular cracks in an oxidized acid environment at room temperature. This room temperature technique is essential in building a library of laboratory-degraded tubes (LDTs) for ECT qualification. For the controlled production of LDTs, direct current potential drop (DCPD) was measured for online crack monitoring [5].

The LDTs were then exposed to PWR's primary or secondary water chemistry environments to form oxide films on the cracked surfaces. In such an environment, electrochemical corrosion potential (ECP) monitoring and electrochemical impedance spectroscopy (EIS) were performed for oxide characterization. Finally, the properties and depth profiles of oxide film were verified by using FE-SEM. The effects of the oxide films on ECT's capability to detect surface IGSCCs in laboratory-degraded alloy 600 steam generator tubing were systematically assessed.

In this study, we focused on the effect of the oxide film on crack size detection. The oxide film on the surface may unintentionally cause the size of the crack to be underestimated. Differences in the measurement data of length and depth of crack appear to be caused by changes in electrical conductivity due to the oxide film. The results of ECT experiment in this paper will help to understand the effect of the oxide film, and it is expected to ultimately contribute to improving the reliability of non-destructive inspection and the structural integrity of the nuclear power plant.

2. Materials and methods

2.1. Properties of the sample tube

A commercial sample of Alloy 600 tubes with 0.025% carbon, produced for nuclear steam generators of the Korean Standard Nuclear Power Plant, was obtained from the Doosan Heavy Industry for this work (Table 1). The tubes had outer diameters of 19.05 mm and wall thicknesses of 1.2 mm, with a microstructure corresponding to a typical high temperature mill annealed alloy (Table 2). These tubes were furnace-sensitized and heat treated at 600 °C for 48 h in a reducing atmosphere to produce a microstructure that was susceptible to IGSCC in aqueous solutions [4,6]. The sensitized tubes were then cracked by exposing them to a 0.1 M aqueous solution of sodium tetrathionate ($Na_2O_6S_4 \cdot 2H_2O$) at room temperature and atmospheric pressure [3].

2.2. Treatment for the surface oxide formation

For the surface oxide formation, the cracked Alloy 600 specimens were exposed to simulated PWR primary water environments inside a high pressure autoclave. The autoclave for the oxide film formation at high temperature and high pressure conditions was constructed using 316L stainless steel with a titanium tank for water chemistry preparation. The head of the water-charging pump was made of titanium, and the balls of the check valves were made of sapphire. All other components exposed to high temperature water, including compression fittings and tubing, were made of 316L. The nominal flow rate to the cell was maintained at 3.8 l/h during experiments.

The chemical conditions of typical PWR primary water were used. Water with a resistivity of 18 MΩ-cm was mixed with chemicals to produce 1,200 ppm boron in the form of boric acid (H_3BO_3) and 2 ppm lithium in the form of lithium hydroxide (LiOH). Water was deaerated by bubbling with nitrogen gas so that the dissolved oxygen (DO) concentration dropped below the limit value of 5 ppb by weight. The operating pressure was about 15 MPa and the temperature was maintained at 320 °C. To simulate the primary side of nuclear PWRs, dissolved hydrogen (DH) ranged from 25 to 30 cm^3 (STP)/kg, about 2.2–2.7 ppm by weight in dissolved form, was maintained in the experiment. Most of the time, dissolved hydrogen was set at 2.65 ppm [7].

2.3. Applied load for crack generation

For the production of a long-shallow axial crack, the radial denting technique was used in this work. Fig. 1 shows a schematic diagram of radial denting techniques applied to form axial cracks at outer or inner wall surfaces. Based on 2D and 3D finite element analyses (FEA) using ABAQUS, the dent loadings of 18.6 kN and 35.6 kN per 1 m of the axial length were applied at the inner and outer walls respectively to obtain 90% of the yield strength. In the case of the outer wall with the maximum applied load, the extent of plastic deformation was predicted using FEA. Diametric changes were predicted for loads up to 35.6 kN/m and for the subsequent unloading. After complete unloading, the residual plastic deformation was predicted to be about 5 μm on the diameter, which was too small to disturb ECT.

A 3D FEA was performed using ANSYS for the direct tensile loading condition, in order to check the adequacy of the stress state and the reliability of the tube specimen design for producing circumferential cracks. Fig. 2 shows a schematic diagram of the circumferential crack production test. From the FEA results and analytic solutions, it is shown that when a tensile load of 14.7 kN is applied to the pin joint, a tensile axial stress of about 200 MPa is to set up uniformly in the crack generation region. This stress value corresponds to 90% of the yield strength of the SG tube.

3. Results

3.1. Production of laboratory degraded steam generator tubes

Based on the supporting conclusions from FEA, dent loading experiments were performed to successfully produce axial cracks at room temperature. A long axial crack, with a total crack length of 17.65 mm, was obtained, as shown in Fig. 3. At each DCPD probe location, the cracked tube was sectioned to confirm the crack depth. Each section was then observed using an optical microscope. The crack depths in the direction of the wall thickness ranged from 0.55 mm to 1 mm. The aspect ratio of outside diameter (OD) axial crack, 17.65 mm long, was calculated to be greater than 16. Because the general aspect ratios of field degraded SG cracked tubes are about 10, the radial denting method is shown to be useful to obtain high aspect ratios.

Cracks were produced on the inner wall using the radial dent loading method. In order to obtain positive proof of inner wall crack generation, an experiment was conducted to confirm the initiation conditions of the cracks using a long focal optical microscope. Fig. 4 shows photographs of cracks that occurred in the test. A 15.5 mm crack and a 9.9 mm crack were assembled to show that a long and shallow crack with a total length of 25.4 mm had been

Table 1
Chemical analysis on Alloy 600 tube.

Chemical	C	Si	Mn	Ni	Cr	P	S	Co	Al	Ti	N	Cu	Fe	B
Weight %	0.025	0.15	0.24	75.47	15.36	0.005	0.001	0.008	0.19	0.29	0.0085	0.023	8.23	0.003

Table 2
Mechanical and metallurgical test results of this SG tube.

Tensile test				Metallographic test			
Temp [°C]	0.2% Y.S. [KSI]	T.S. [KSI]	E [2"]	ASTM grain size	Roughness	Hardness-ID	Corrosion rate
20	38.5	91.5	47	4.0–5.0	17.70 - OD 9.60 - ID	68	13

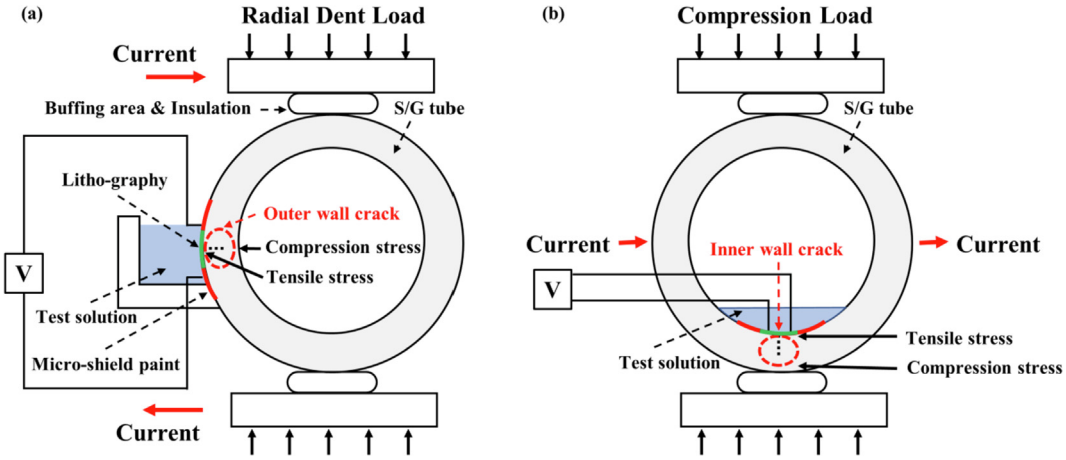

Fig. 1. Radial denting methods for introducing axial cracks at outer or inner surfaces. (a): Outer surface, (b): Inner surface.

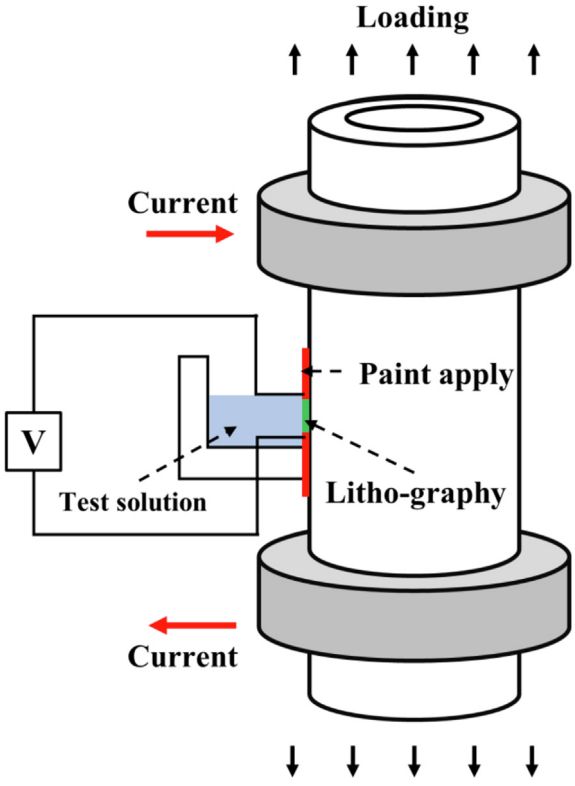

Fig. 2. Outside diameter (OD) circumferential crack with direct current potential drop (DCPD).

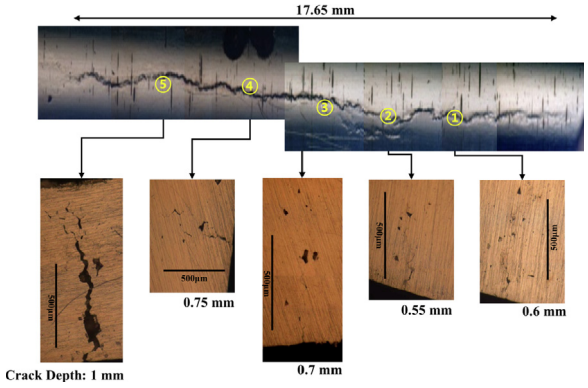

Fig. 3. Destructive examination of a 17.65 mm-OD long and shallow crack and sectioned area for confirming the crack depth (the numbers represent locations of DCPD probes).

generated. The cracked tube was then sectioned using a low-speed metallographic saw to confirm the crack depth at each of the DCPD probe positions. The observed crack depths ranged from 0.8 mm to 1.1 mm.

A few research groups have succeeded in the production of LDT circumferential cracks by using tensile loads [8]. From the reports of these research groups, tension loading is expected to be convenient and inexpensive for the production of cracks. Only the design of the jig for loading differs in this work from those of the other research groups. Based on FEM analysis, circumferential crack generation is expected to be feasible. In the first direct tensile loading test, a crack was detected at the design test load corresponding to 90% of the yield strength after about 80 h of immersion. The measured circumferential crack had a length of 8 mm and a maximum depth of 0.82 mm.

3.2. In-situ DCPD monitoring

To control and monitor the initiation and propagation of cracks, the switching DCPD method was introduced for the tube specimens. The switching DCPD technique is well established and widely used in the field of fracture mechanics [5]. It consists of direct current supply, a solid-state current switching circuit, and a

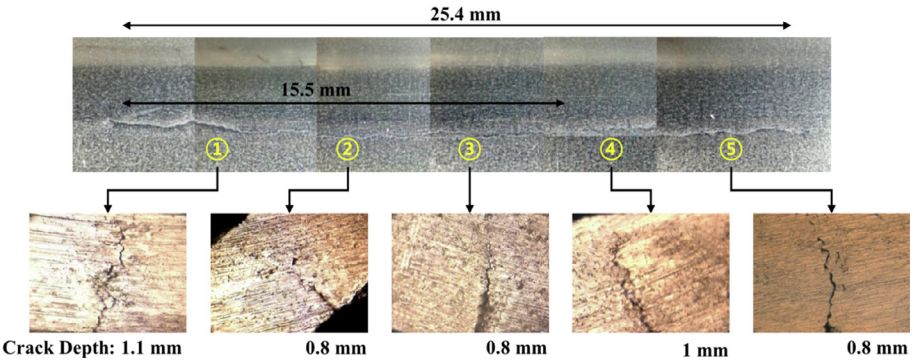

Fig. 4. Destructive examination of a 25.4 mm-OD long and shallow crack and sectioned area sectioned area for confirming the crack depth (the numbers represent locations of DCPD probes).

high-precision voltmeter. The direction of the current flow is periodically alternated by the solid-state circuit to obtain DCPD signals in both directions, and the thermoelectric electromagnetic field noise is then filtered out from the genuine signal.

This DCPD signal is utilized to stop cracking at the desired depth and length either at the inner or outer wall of steam generator tubes. To this end, the DCPD were measured at several locations along the crack length using an array of probes in order to monitor the shape and position of the crack. Fig. 5 shows a comparison of the measured DCPD signal with the predicted signal using FEA for a 25.4 mm long axial crack on inner surface of the tube. At the same crack depth, the two data sets had a consistent difference in DCPD of about 7–9 μV. As the crack depth increased, the measured DCPD signal increased more rapidly in a similar pattern but with a greater slope, which was beneficial for measurement.

For the circumferential crack test, the DCPD online monitoring technique was found to be feasible for controlling the crack depth and length. As shown in Fig. 5, measured DCPD data tended to increase slowly with crack growth. In the case of no crack production in the SG tube, the measured DCPD value was about 25 μV. The DCPD increased to 58 μV after a 0.82 mm deep crack was produced, showing adequate sensitivity. In addition, for the range of experiments, there appeared to be a good correlation between the measured and simulated DCPD data. The difference between the two data for the final crack depth was about 13 μV, which appeared to increase with further crack growth.

In all cases of axial and circumferential cracks, experimental DCPD data of final crack depth at each DCPD probe location were slightly different from the predicted DCPD value. However, as shown in Fig. 6, the predicted depth distribution at each location agrees well with the real depth distribution confirmed from the graphical analysis.

3.3. Surface oxide film formation in PWR primary water chemistry

Recorded test conditions including temperature, pressure, conductivity, DO, and DH are shown in Fig. 7. DH was constant at 30 cc/kg for the first 15 days from the test startup. In order to confirm the effects of the change of DH contents on the rate of change of oxide thickness, DH reduced to 1.5 cc/kg and finally to 0 cc/kg, and then the nominal conditions were recovered near the end of test.

Theoretical pH of the solution at high temperature was calculated using MULTEQ-REDOX Ver.2.22 at several temperatures. MULTEQ code is a commercially available software developed by EPRI, and it is used for calculating pH and the boiling point in high temperature aqueous environments. Only boric acid and lithium hydroxide are considered in the calculation. Table 3 shows the calculated pH in high temperatures with the fitting formula:

$$pH = -26.115 + 0.19968T - 0.00041437T^2 + 2.9081 \times 10^{-7}T^3 \quad (1)$$

where T is the absolute temperature in K for T > 423 K.

In this study, two reference electrodes, $Cu/Cu_2O/ZrO_2$ electrode and Pt (AUEN), were used for measuring the electrochemical corrosion potential (ECP) of Alloy 600 specimen. The $Cu/Cu_2O/ZrO_2$

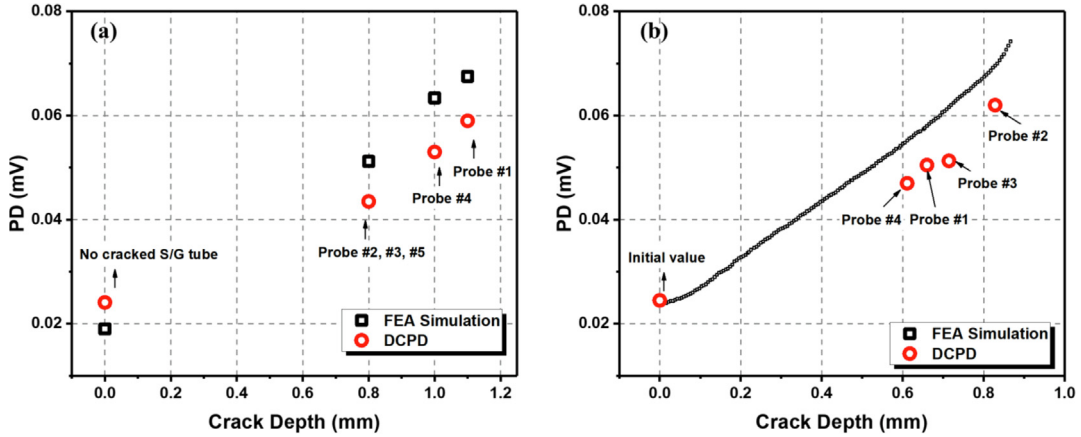

Fig. 5. Comparison of measured and predicted DCPD signals (the numbers represent locations of DCPD probes). (a): Inside diameter (ID) axial crack, (b): Outside diameter (OD) circumferential crack.

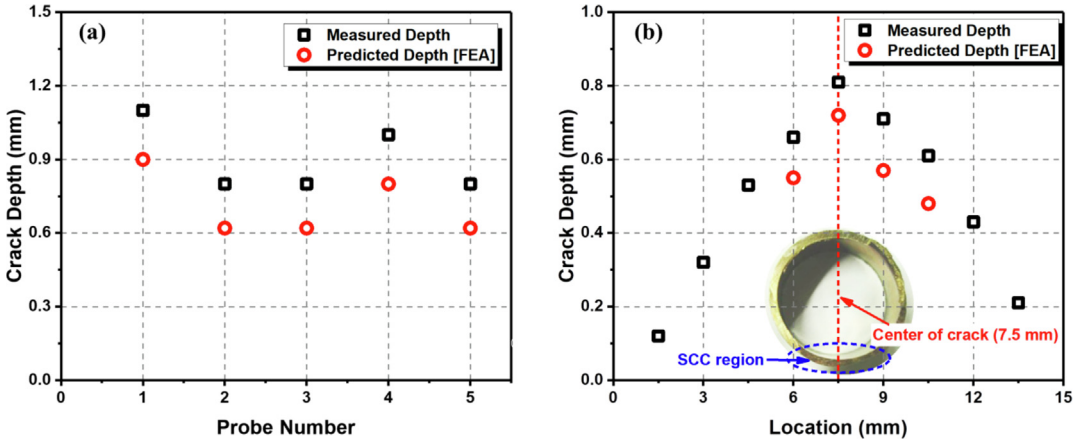

Fig. 6. Measured and simulated depths of axial and circumferential cracks. (a): Axial crack, (b): Circumferential crack.

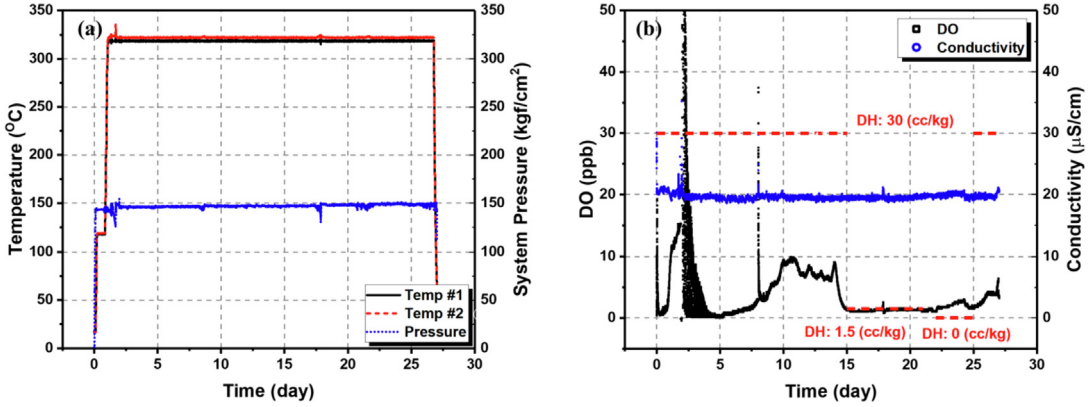

Fig. 7. Test conditions of mockup system for typical PWR primary water. (a): System temperature and pressure, (b): Water chemistry condition.

Table 3
Test water pH at temperature as predicted by MULTEQ-REDOX ver 2.22.

Temperature (K)	25	150	175	200	225	250	275	288	300	320	325
pH	6.42	6.22	6.32	6.40	6.48	6.58	6.73	6.84	6.96	7.22	7.31

electrode has been a very widely used pH sensor for high temperature aqueous environments since its development by Niedlach [9]. Zirconia membrane acts as an oxygen vacancy conductor in the temperature range above about 150 °C [9,10]. In general, 7–8% yttria (Y_2O_3) is added to stabilize zirconia for membrane materials. The zirconia tube with one-end-closed is connected to the autoclave head using a sealing structure and compressive fitting. Cu/Cu_2O reference junction is placed inside the zirconia tube. The half-cell reaction is given as:

$$Cu_2O(s) + 2H^+(aq) + 2e^- = 2Cu(s) + H_2O(l) \quad (2)$$

where the suffix *s*, *aq*, and *l* denote solid, aqueous ionic state, and liquid, respectively.

The electrode potential versus the standard hydrogen electrode, SHE, can be expressed as:

$$E = E^o - \frac{RT}{2F}\ln\frac{1}{[H^+]^2} = E^o - \frac{2.303RT}{F}pH \quad (3)$$

Standard electrode potential E^o at the unit activity of H^+ versus SHE can be calculated by utilizing thermodynamic data. A polynomial fitting results in:

$$E^o = 0.62262 - 0.00056175T + 1.938 \times 10^{-7}T^2 \quad (4)$$

The platinum counter electrode for the electrochemical measurements in the experiment was in the form of a 0.5 mm wire that was sealed with a heat shrinkable PTFE tube, and except for the top reaction area, was connected through a CONAX® fitting. The electrode surface of the reactive area was platinized to exemplify the actual reaction area. The half-cell electrode potential on the platinum surface is:

$$2H^+(aq) + 2e^- = H_2(g) \quad (5)$$

Taking E_0 to be zero, the electrode potential versus SHE is given by:

$$E = E^o - \frac{RT}{2F}\ln\frac{f_{H_2}}{[H^+]^2} = -\frac{RT}{2F}\ln f_{H_2} - \frac{2.303RT}{F}\log\frac{1}{[H^+]} \quad (6)$$

Fugacity of hydrogen was approximated as Henry's constant

times the mole fraction of hydrogen in the solution. From the experimental data, Henry's constant for hydrogen is usually given in the form H = a + b/T [11].

$$H = 21.13 \times 10^4 - 4.20 \times 10^7 \Big/ T \; for \;\; 293.15 < T < 298.15 \quad (7)$$

$$H = -9.01 \times 10^4 + 5.83 \times 10^7 \Big/ T \; for \;\; 393.15 < T < 547.15 \quad (8)$$

Equation (6) may be reduced to

$$E = -\frac{RT}{2F}\ln Hx - \frac{2.303RT}{F}pH = -\frac{RT}{2F}\left[\ln\left(a + \frac{b}{T}\right) + \ln x\right] - \frac{2.303RT}{F}pH \quad (9)$$

The working electrode was manufactured according to the following. Alloy 600 SG tubing materials were cut by EDM into rectangular shapes (10 × 10 mm) with the original tube curvature. Specimens were carefully polished to eliminate all the oxide layer produced by EDM cutting. These were then spot-welded to alloy 600 wires of 0.5 mm diameter, which were sealed by heat shrinkable PTFE tube. CONAX® fitting was used to connect the electrodes through the autoclave. The difference between ECP of the two electrodes was measured to be about 0.3 V at 320 °C.

3.4. Surface oxide film formation in PWR secondary water chemistry

For the surface oxide formation, Alloy 600 specimens were also exposed to simulated PWR secondary water environments inside a high-pressure static cell. The cell, for the in-situ observation at high temperature and high pressure conditions, was constructed with a custom-designed one gallon-capacity Ni-200 autoclave. The alkaline tube sheet crevice water-chemistry condition of PWR SG was simulated with 10 wt% NaOH solution deaerated with 5% hydrogen gas with nitrogen balance [11]. The temperature increased from room temperature to 315 °C.

4. Discussion

4.1. Electrochemical impedance spectroscopy (EIS) in PWR primary water chemistry

A plate shaped working electrode of 1 cm^2 area was first polished with wet SiC paper of decreasing grit size (400, 600 and up to 1000) and was then polished with alumina (3 μm). It was finally ultrasonically cleaned in distilled water and then dried in air. The AC impedance scan frequencies ranged from 10^6 to 10^{-1} Hz, and the spectra were collected using a computer-driven system consisting of a Solartron 1260 frequency response analyzer, a Solartron 1286 potentiostat, and a Zplot® software. The experimental data were interpolated with a Solartron Zview software to model the best equivalent circuit for approximating the impedance behavior.

EIS was applied to monitor the oxide thickness during exposure in the autoclave. The oxide film worked as a capacitor with a low dielectric constant. Because we were able to measure the capacitance of the oxide using EIS, the thickness of the oxide was calculated by Eq. (10) [12]:

$$C = \varepsilon \cdot \varepsilon_0 \cdot \frac{A}{d} \quad (10)$$

where C is the measured capacitance (Farad), A is the specimen surface area (m^2), d is the oxide thickness (m), ε is oxide dielectric constant, and ε_0 is 8.854 × 10^{-12} F/m.

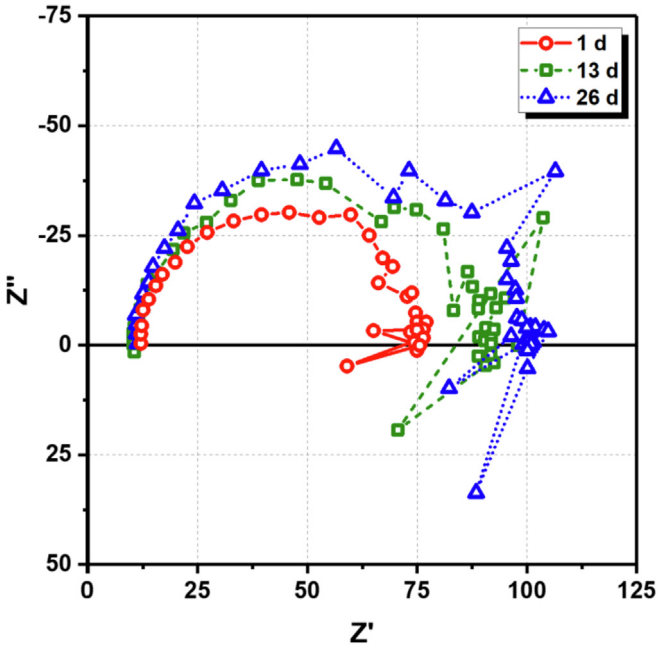

Fig. 8. Complex Nonlinear Least Square fitting of Alloy 600 in PWSCC environment.

A typical semi-circular complex impedance diagram was obtained for the formation of oxides on the surface [12]. Fig. 8 shows the EIS results of Alloy 600 in PWSCC environment. The radius of the semi-circular impedance signal gradually increased with time. The Equivalent Circuit Analysis (ECA) can be used to analyze the EIS signals. Complex Nonlinear Least Square (CNLS) fitting was performed for each of the EIS data [9]. The fitted values of the oxide resistance and capacitance are shown in Table 4. The oxide thickness at each state can be determined by using Eq. (10). These values are later to be compared with the measured thickness.

4.2. FE-SEM results for oxide films

The inner and outer walls of the cracked LDT Alloy 600 specimens were installed in the autoclave, and oxidized in PWR primary condition with circulated water at 320 °C and 15 MPa for about 30 days. In the alkaline secondary crevice condition with 10 wt% NaOH solution, the LDTs were exposed at 315 °C for about 10 days. After oxidation at each water chemistry condition, the surfaces and cross sections of the Alloy 600 specimens were examined using a combination of JEOL® Model JSM-6330F Field Emission Scanning Electron Microscope (FE-SEM) to identify the oxide phase and to characterize their morphology and thickness.

For cross-sectional analysis, the exposed specimens were carefully prepared. A thin film of platinum was sputter-coated, and nickel was electrolytic plated on the specimens to prevent the oxide layer from possible damage. The plating conditions are given in Table 5. After the two-step plating, the specimens were embedded into a epoxy, and their cross sections were then polished

Table 4
Oxide properties and thickness measured by EIS.

Measurement time (mm/dd)	12/01	12/13	12/26
Oxide resistance (Ω)	62.61	76.13	87.01
Oxide capacitance (μF)	0.47087	0.45558	0.45249
Oxide thickness (μm)	0.18803	0.19435	0.19567

Table 5
Au and Ni plating condition.

Method	Medium	Electrode	Current (mA)	Temperature	Thickness
Electrolytic	$NiSO_4$+$NiCl_2$+H_3BO_3	Pure Ni	10	Room Temp.	few μm
Sputtering	Vacuum: 0.05–0.2 Torr	Pure Au	10	Room Temp.	5 nm/min

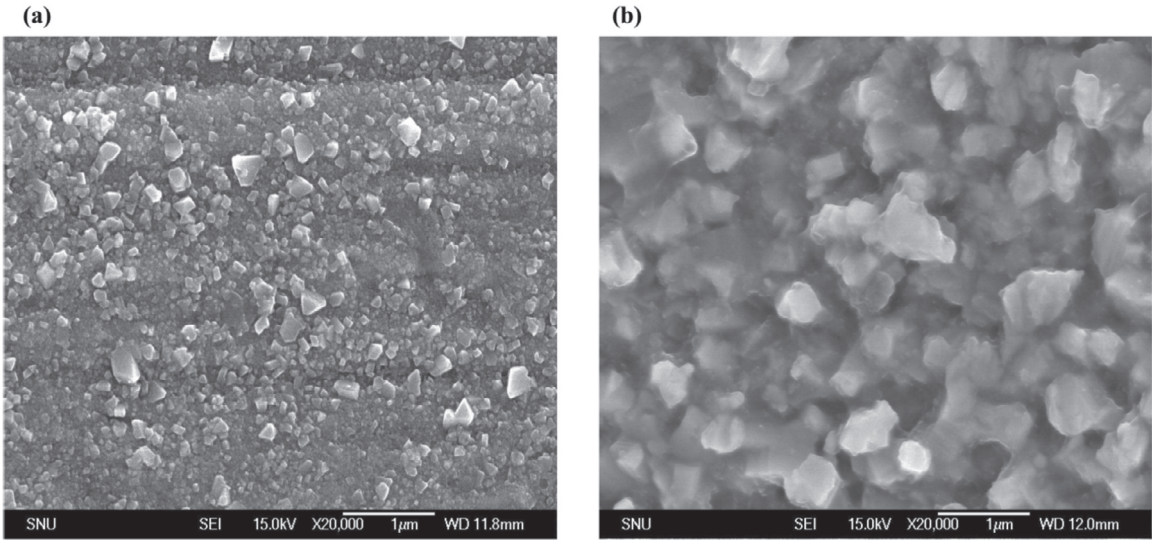

Fig. 9. FE-SEM micrographs of the surface of specimens oxidized in (a) primary and (b) secondary environment.

mechanically by first using SiC papers and then AlO_3 powder (0.1 μm). Oxide surface examination was made after platinum coating without Ni-plating. Fig. 9 is FE-SEM micrographs of surfaces oxidized in primary and secondary environments, respectively. FE-SEM photo-micrographs at higher magnifications, shown in Fig. 9, indicated that platelet forms appear to grow into polyhedral known as Ni–Fe spinel oxide ($NiFe_2O_4$) [13].

FE-SEM micrographs of cross-sectional specimens oxidized in primary and secondary environments are shown in Fig. 10. The cross-section of the oxide layer was revealed between Alloy 600 substrate at the bottom and the Ni-plating at the top. The mean thickness of the oxide layers on the specimens oxidized in the primary environment was about 350 μm. This measured value is about 1.5 times the thickness predicted by EIS. In the case of cross-sectional samples oxidized in the secondary environment, the thickness of the oxide layers was measured to be about 700 μm, which is about twice the measured thickness in the primary water.

4.3. Effect of oxide film on ECT's capability to detect surface IGSCC in LDT

All the fabricated LDTs were subjected to two separate ECTs to examine the crack depth and length before and after oxidation. A total of six LDT specimens, including OD axial and circumferential, and ID axial and circumferential cracked tubing specimens, were used. The first ECT experiment was performed by the NDT Center at the Korea Electric Power Research Institute (KEPRI). The crack depth and length were measured with a 300 kHz C-scan with a phase angle curve estimation using the point coil channel of ECT facility [14]. The C-scan pictures of the first ECT results were shown in Figs. 11 and 12 for axial and circumferential cracks, respectively. The second ECT experiment was performed for the oxidized LDTs that passed the first ECT. To avoid hardware variability, the second ECT was performed at the same institute using the same hardware but with a different operator.

For easier comparison, the ECT results before and after oxidized treatment on the same LDT sample are shown in the top and

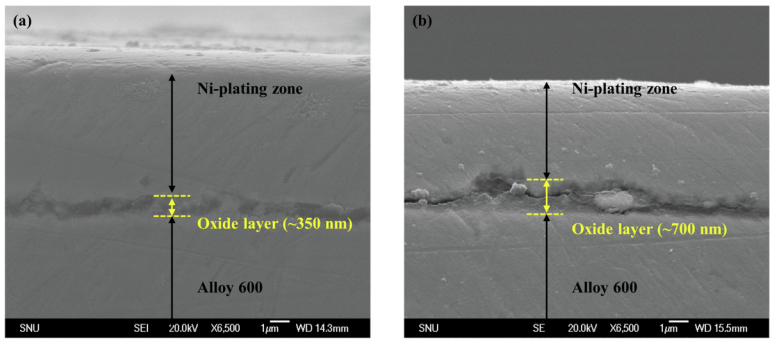

Fig. 10. FE-SEM micrographs of cross section of oxidized specimens oxidized in (a) primary and (b) secondary environment.

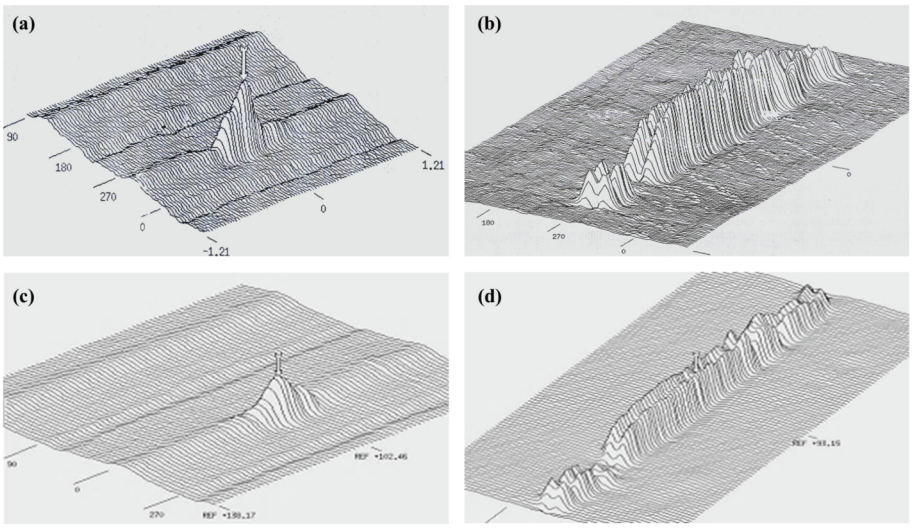

Fig. 11. ECT results before and after oxidized treatment on axial cracked LDT sample. (a): OD axial crack w\o Oxide film, (b): ID axial crack w\o Oxide film, (c): OD axial crack with Oxide film, (d): ID axial crack with Oxide film.

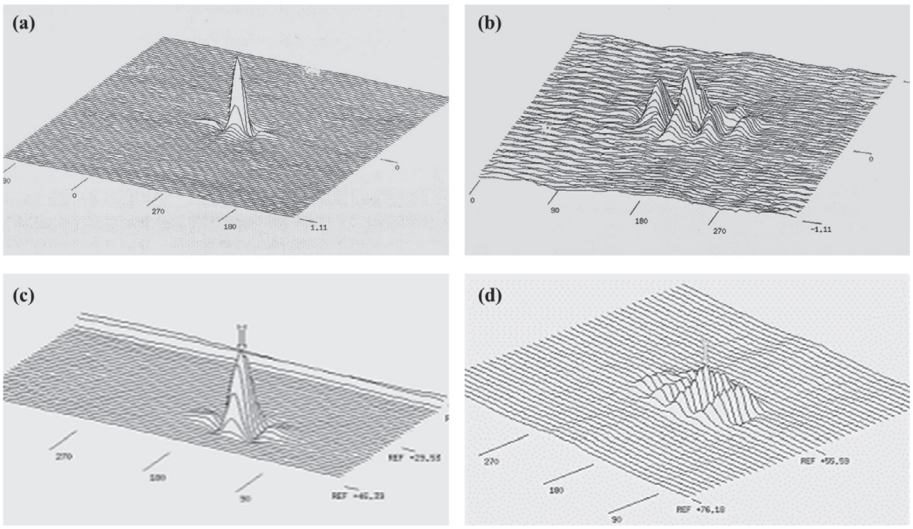

Fig. 12. ECT results before and after oxidized treatment on circumferential cracked LDT sample. (a): OD circumferential crack w\o Oxide film, (b): ID circumferential crack w\o Oxide film, (c): OD circumferential crack with Oxide film, (d): ID circumferential crack with Oxide film.

bottom of Figs. 11 and 12. As shown in the Figures, the C-scan peak tends to be blunted after the oxidized treatment. A quantitative analysis of all the ECT results is summarized in Table 6 with Fig. 13. In these, the crack depth is represented as the percentage of tube through a wall thickness of 1.2 mm. Except for one of the cases in the ID axial crack that extended beyond the maximum DCPD probe range (25 mm), all other cases show remarkable agreement between ECT and DCPD.

As shown in Table 6, except for the case of a long ID axial crack length, the crack shape, predicted by DCPD, is also almost the same as the estimates given by ECT in the absence of an oxide film. In the case of circumferential cracks, the DCPD underestimated the crack depth and length by 20–30% compared with ECT values. In the axial crack cases, the difference between the two measurement methods was less than 15%.

As noted by the ECT C-scan results, the surface oxide film is shown to make an important impact on ECT's detection capabilities, as confirmed by Fig. 13. For cracks whose growth did not penetrate through the tube wall, similar underestimations were made on ECT by the surface oxide. This led to ECT's underestimation by 24% in length and 17% in depth for the OD axial crack, and 7% in length and 24% in depth for the ID circumferential crack due to oxide films. The degree of underestimation decreased with an increase in the crack length. The electric conductivity of the oxide film may be the major factor that affects the ECT results. Cr-oxide has electrical insulating properties, so it has a positive effect on measuring the depth of cracks in non-destructive testing using electro-magnetic devices such as an ECT method. In contrast, it was reported that the electric conductivity of the oxide film increases when Ni-based alloy exists in it [15]. Thus, under experimental conditions where Ni–Cr spindle oxide and Ni/Cr oxide film coexist, the effect of Ni increases the conductivity of the oxide film. The measured size of crack with oxide film using the ECT method could be smaller than that of crack without oxide film.

Table 6
Effect of oxide film on ECT detectability.

		ECT Results		DCPD Result (w/o oxide film)
		w/o oxide film	with oxide film	
ID Axial (primary)	Length	99.9 mm	96.3 mm	>25 mm[a]
	Depth	99%	98%	95.67%
OD Axial (secondary)	Length	15.5 mm	11.8 mm	13 mm
	Depth	88%	73%	83.3%
ID Circumferential (primary)	Length	127°, 18.5 mm	117°, 17.2 mm	90°, 13.1 mm
	Depth	87%	66%	75%
OD Circumferential (secondary)	Length	25°, 3.8 mm	21°, 3.5 mm	20°, 3 mm
	Depth	99%	98%	79.2%

[a] Crack length exceeds the maximum range (25 mm) of DCPD prove coverage.

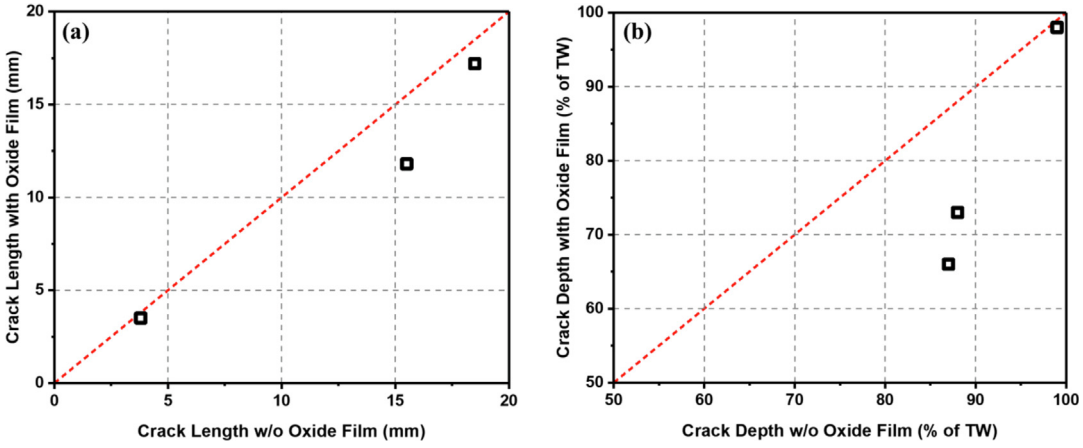

Fig. 13. Oxide film effect on the crack prediction by ECT. (a): Length, (b): Depth.

5. Conclusion

In order to produce a library of Laboratory-Degraded SG Tubes (LDT) made of Alloy 600 with intergranular cracks, a radial dent loading method and a direct tension loading method were developed as advanced techniques for accurate crack size control and for enhanced productivity. The experimental and FEA of this new IGSCC mockup technique was shown to be reliable and time-saving. The room temperature mockup crack can be monitored and controlled online using a switching DCPD with array probes. The DCPD method was demonstrated to be applicable and adequate for both the radial dent and the direct tension loading methods. FEA was performed for the validation and sensitivity evaluation of the DCPD method. Using the LDT production procedures, it was found that the crack length and depth predictions, as well as the DCPD measurements, agreed well with the crack size estimations given by ECT in the absence of an oxide film. The oxide film was found to be an important cause of crack size underestimation by ECT. It was also found that the oxide film is conducive to DCPD's underestimation of crack size.

Acknowledgements

This work was financially supported by the Major Institutional Project of Korea Institute of Machinery and Materials (KIMM) funded by the Ministry of Science and ICT (No.NK220C) and the Human Resources Development of the Korea Institute of Energy Technology Evaluation and Planning (KETEP) grant funded by the Korea Government Ministry of Trade Industry and Energy (MOTIE) (No. 20194030202400).

References

[1] M. Kemppainen, I. Virkkunen, J. Pitkänen, R. Paussu, H. Hänninen, Nucl. Eng. Des. 224 (2003) 105.
[2] J. Wåle, Crack characterisation for in-service inspection planning-an update (No. SKI-R–06-24), Swedish Nuclear Power Inspectorate, 2006.
[3] I.S. Hwang, Embitterment Mechanisms of Nickel-Base Alloys in Water, Ph.D. Thesis, MIT, Massachusetts, 1987.
[4] T.H. Lee, I.S. Hwang, H.S. Chung, J.Y. Park, J. Press. Vessel Technol. 130 (2008) 1.
[5] ASTM, Standard Test Method for Measurement of Fracture Toughness (E1820-01), American Society for Testing and Materials, Annual Book of ASTM Standards, West Conshohocken, PA, 2001.
[6] I.S. Hwang, S.U. Kwon, S.G. Lee, J.H. Kim, Corrosion 57 (2001) 787.
[7] S.H. Oh, In-situ EIS of Oxide Film Formed on Nickel-Plated Alloy 600, M.S. Thesis, Seoul National University, Seoul, 2002.
[8] D.R. Diercks, S. Bakhtiari, K.E. Kasza, D.S. Kupperman, S. Majumdar, J.Y. Park, W.J. Shack, Steam Generator Tube Integrity Program: Annual Report (NUREG/CR-6511), U.S. Nuclear Regulatory Commission, Washington, D.C., 1999.
[9] L.W. Niedrach, J. Electrochem. Soc. 129 (1982) 1445.
[10] L.W. Niedrach, W.H. Stoddard, Corrosion 41 (1985) 45.
[11] D.M. Himmelblau, J. Chem. Eng. Data 5 (1960) 10.
[12] M.E. Orazem, B. Tribollet, Electrochemical Impedance Spectroscopy, Wiley-Interscience, New York, 2008.
[13] P. Combrade, P.M. Scott, M. Foucault, E. Andrieu, P. Marcus, Oxidation of Ni base alloys in PWR water: oxide layers and associated damage to the base metal, in: 12th International Conference on Environmental Degradation of Materials in Nuclear Power System, Salt Lake City, Utah, August 14-18, 2005.
[14] EPRI, Steam Generator Eddy Current Data Analysis Performance Demonstration, Electric Power Research Institute, Palo Alto, 1995.
[15] M. Linder, T. Hocker, L. Holzer, O. Pecho, K.A. Friedrich, T. Morawietz, R. Hiesgen, R. Kontic, B. Iwanschitz, A. Mai, J.A. Schuler, Solid State Ionics 283 (2015).